Galvin, K.P. & Dickinson, J.E. 'Fluidized bed desliming in fine particle flotation - Part II Flotation of a model feed', Chemical Engineering Science, 108, 299-309 (2014)

Available from: http://dx.doi.org/10.1016/j.ces.2013.11.027

Author's Accepted Manuscript

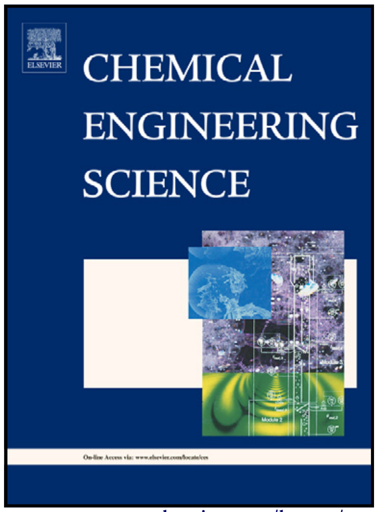

Fluidized Bed Desliming in Fine Particle Flotation – Part II Flotation of a Model Feed

K.P. Galvin, J.E. Dickinson

PII: S0009-2509(13)00763-X
DOI: http://dx.doi.org/10.1016/j.ces.2013.11.027
Reference: CES11407

To appear in: *Chemical Engineering Science*

Received date: 5 August 2013
Revised date: 10 November 2013
Accepted date: 14 November 2013

Cite this article as: K.P. Galvin, J.E. Dickinson, Fluidized Bed Desliming in Fine Particle Flotation – Part II Flotation of a Model Feed, *Chemical Engineering Science,* http://dx.doi.org/10.1016/j.ces.2013.11.027

Fluidized Bed Desliming in Fine Particle Flotation

– Part II Flotation of a Model Feed

K.P. Galvin and J.E. Dickinson[1]

Centre for Advanced Particle Processing and Transport, Newcastle Institute for Energy and Resources, The University of Newcastle, Callaghan, NSW 2308, Australia

Abstract

This is the second in a series of papers concerned with the performance of a novel technology, the Reflux Flotation Cell. Part I examined the system hydrodynamics, commencing with a gas-liquid system and examination of the fluidization boundary condition. The desliming, or potential to reject entrained fine gangue particles from the product overflow, was investigated by introducing hydrophilic particles. In Part II, a model feed consisting of hydrophobic coal particles and hydrophilic silica was introduced. The separation of these two components was investigated across an extreme range in the applied gas and wash water fluxes, well beyond the usual limits of conventional flotation.

The Reflux Flotation Cell challenges conventional flotation cell design and operation in three ways. Firstly, the upper free-surface of the flotation cell is enclosed by a fluidized bed distributor in order to fluidize the system in a downwards configuration, counter-current to the direction of the rising air bubbles. Secondly, a system of inclined channels is located below the vertical section of the cell, providing a foundation for increasing bubble-liquid segregation rates. Thirdly, the system is operated with a bubbly zone, hence in the absence of a froth zone. This combination of conditions provides for the establishment of a high volume fraction of bubbles in the bubbly zone, of high permeability, ideal for promoting enhanced counter-current washing of the rising bubbles, and hence high quality desliming. The

[1] Corresponding author: Tel: +61 2 4033 9088; Fax: +61 2 4033 9095.
E-mail address: Jamie.Dickinson@newcastle.edu.au

arrangement permitted operation at extreme levels in the value of the fluidization (wash water) flux and the gas flux, with the fluidization flux set at up to 2.1 cm/s and the gas flux set at up to 4.7 cm/s for a mean bubble size, d_b, of 1.5 mm. These gas and wash water fluxes corresponded to a bubble surface flux of 188 $m^2/m^2.s$ and a positive bias flux of 1.7 cm/s. Thus the operating regime was shown to be far broader than that achieved by conventional flotation, thereby confirming the robust nature of the system. The model flotation feed provided a basis for establishing the flotation performance across this vast regime of operation. Full combustible recovery of fine coal and full rejection of mineral matter were achieved, with good agreement with the Tree Flotation curve. At extreme levels of wash water addition it was possible to selectively strip poorer floating coal particles from the bubble surface, and in turn achieve beneficiation results significantly better than those defined by the Tree Flotation method.

Keywords: Flotation, Desliming, Drift Flux, Inclined Channels, Fluidization, Froth

1. Introduction

While flotation is very much a physiochemical process, the hydrodynamics play a critical role in effecting the final overall separation (Jameson, 2012; Massinaei et al., 2009; Neethling and Cilliers, 2001). Indeed, once the hydrophobic particles have been attached to the air bubbles, flotation can be considered as a separation between relatively large low density entities called air bubbles, and relatively fine high density particles referred to as gangue (George et al., 2004). Thus the final stage of flotation can be described as a simple gravity separation process. Our recent advances in gravity separation, based on the development of the Reflux Classifier, have therefore been extended to flotation to promote more effective desliming of the flotation product. The novel flotation arrangement, which is shown in Figure 1, is a modified, inverted Reflux Classifier (Galvin et al., 2012; 2010). This inverting of the Reflux Classifier results in a device known as the Reflux Flotation Cell that is ideal for recovering particles less dense than water, namely air bubbles and their associated hydrophobic particles, while rejecting the hydrophilic particles through the introduction of fluidization water. It is emphasized that this arrangement is fundamentally different to the HydroFloat (Zang et al., 2004) which is not designed to provide any form of desliming (rejection of entrained fine gangue particles), given the application of conventional fluidization from below the system.

The Reflux Flotation Cell, shown in Figure 1, is also very different to traditional flotation devices. Firstly, the upper free-surface of the flotation vessel is enclosed by a water fluidization distributor. Effectively, the system is an inverted fluidized bed. A central discharge point is provided for recovering the bubbly flow product out the top. Consequently, unlike in traditional flotation vessels in which typically 80% of the gas flux disengages from the bubbly product via the free-surface (Neethling and Cilliers, 2001), all gas exiting the Reflux Flotation Cell is directed to flow with the product overflow. The feed and the gas are introduced via a downcomer, described in more detail in the Experimental Section. A second feature of the device is the system of parallel inclined channels below the main vertical section. The inclined channels increase the rate of segregation between the air bubbles and the liquid, preventing the air bubbles from being entrained towards the tailings outlet. This feature is an application of the Boycott Effect (Boycott, 1920), and is especially important when large fluidization (wash water) fluxes and gas fluxes are imposed. Thirdly, this system is best operated using a concentrated bubbly zone rather than a froth zone. A concentrated bubbly zone, which forms naturally beyond the flooding condition, is very permeable compared to a froth zone (Lorenceau et al., 2009; Rouyer et al., 2010), and hence ideal for applying very high fluidization water fluxes.

Dickinson and Galvin (2013) have previously described this novel flotation arrangement. The focus of their previous study was on the washing of fine silica particles from a bubbly-froth product, in the absence of any hydrophobic particles. A very resilient gas-liquid interface, formed from the surfactant sodium dodecyl sulfate (SDS), was used in order to produce relatively fine gas bubbles of order 340 microns in diameter, and prevent bubble coalescence. As noted, there were no hydrophobic particles used in the first study. The fine silica particles used in the study, which were nominally 5 to 22 microns, were hydrophilic. These particles were nevertheless forced to interact with the air bubbles within the high shear rate field of the downcomer. These conditions were designed to produce a system that would firstly entrain the slimes, and in turn be difficult to deslime. With the very fine gas bubbles, the foam drainage rates are relatively low, while there is an increased tendency for water to be entrained into the product. Their work demonstrated the potential to operate at a very high bubble surface flux, $S_b = 6j_g/d_b$, of 144 $m^2/m^2.s$, well beyond the flooding condition, while rejecting up to 99% of the hydrophilic slimes.

Our new paper presents the findings on a more realistic system with a model flotation feed consisting of hydrophobic particles of fine coal and an equal mass portion of fine silica. The purpose of the study was to determine the potential boundaries of the new system through the application of extreme levels of fluidization and imposed gas fluxes. Thus a range of operating conditions, varying from those more typically used in industry to extreme, beyond-flooding, were applied in order to assess the robustness of the system. The system was evaluated by quantifying the recovery of the hydrophobic particles and the rejection of the fine silica from the product. The model flotation feed consisted of fine coal that had been previously recovered by industry using flotation. Hence it was possible to bench-mark the performance of the Reflux Flotation Cell against conventional flotation, in the presence of a well-defined and significant portion of fine silica. A more appropriate frothing agent for recovering fine coal, methyl isobutyl carbinol (MIBC), was used at a moderate dosage of 20 ppm. This reagent tends to produce larger bubbles and weaker froths, and hence a system that is more susceptible to the effects of coalescence.

The present study is significant because it challenges the traditional approach to flotation. Figure 2 shows the typical operating regime of conventional cells, with the wash water flux plotted versus the gas flux. For the relatively large bubble sizes used in the present study, with the diameter ranging from 0.5 to 3 mm, the gas flux, j_g, is typically limited to between 0.6 and 1.5 cm/s, producing bubble surface area fluxes between 30 and 60 $m^2/m^2.s$ (Fuerstenau et al., 2007; Massinaei et al., 2009). While larger values can be used, approaching perhaps 2.0 cm/s, there is an increased tendency for the interface between the bubbly zone and the froth to disappear, leading to difficulties in process control of the interface elevation, loss of bubbles to tailings, and very high liquid entrainment rates containing slimes reporting with the froth to the product. Wash water, with fluxes ranging from 0.05 cm/s up to 0.4 cm/s, and sometimes moderately higher, are used to assist with the washing of the froth (Fuerstenau et al., 2007; Yianatos et al., 1987).

Figure 2 also places the new work into perspective by showing the conditions used in the present study. The operating regime used here is vastly larger than has, arguably, ever been applied in the past. This systematic study thus establishes the hydrodynamic boundaries of the Reflux Flotation Cell at levels that go well beyond any conventional system. This study assesses the system performance at this boundary. Moreover, an independently determined Tree Flotation analysis, conforming to the Australian Standard AS4156.2.2, was completed to provide a further basis for assessing the separation performance.

2. Theory

In this section the steady state transport of gas bubbles and liquid in a vertical column is described. All system inputs and outputs are defined as positive values, and all vector quantities are defined as positive in the upwards direction apart from the bias flux, j_b, which is positive downwards. Dickinson and Galvin (2013) have drawn an important but subtle distinction between injecting the wash water at a position just below the upper surface, and injecting the wash water from above the upper surface. Clearly the two cases can differ by a mere infinitesimal amount, but the theoretical consequences can be very large.

If the water is injected at a position well below the upper surface then, according to Drift Flux theory, foam rising above this position effectively reforms and establishes itself in a manner that is identical to that which occurs in the absence of any wash water injection. Dickinson and Galvin (2013) considered what happens when we gradually raise the elevation of the wash water injection. The zone between the injection point and the upper surface retains this same fixed state, regardless of how narrow the zone becomes, even when it becomes infinitesimal. But when the injection point shifts from just below the upper surface to an elevation that coincides with the upper surface, the system then becomes formally fluidized. There is a subtle but significant theoretical distinction between these two cases. They show that when the system is formally fluidized all of this fluidization water is, in some cases, transferred directly to the product, delivering no desliming.

The recent study by Dickinson and Galvin (2013) established the correct fluidization boundary condition of the Reflux Flotation Cell system. Although the fluidization water is introduced at the upper system boundary, the system behaves as though the fluidization wash water enters a finite distance below the upper system boundary. Thus, in analysing the Reflux Flotation Cell it is appropriate to assume the wash water addition is introduced below the upper interface. This wash-water fluidization leads to the generation of positive bias, and hence strong desliming.

Figure 3 provides a schematic representation of (A) a conventional flotation system without the use of wash water, and (B) the upper section of the Reflux Flotation Cell. The introduction of the fluidization flux, j_w, in the Reflux Flotation Cell is assumed to occur at some finite distance below the upper surface. It is necessary for a theoretical examination of both the zones above and below this entrance level. This consideration is theoretically necessary despite the fact that the zone above the fluidization (wash) water entrance is effectively negligible in height. Above the fluidization entrance level the upwards liquid flux is j_f, and the volume fraction of bubbles is θ_b. Below the entrance level the bias flux, j_b, is defined as positive in the downwards direction. Here, $j_b = j_w - j_f$. The corresponding volume fraction of bubbles below the wash water entrance level is θ_w, and volume fraction of liquid is θ_L. The total flux passing up through any horizontal layer in the zone between where the fluidization water enters, and where the gas enters is,

$$\psi_T = j_g - j_b = j_g + j_f - j_w. \tag{1}$$

The total flux is also given by the sum of the bubble and liquid flux,

$$\psi_T = u_b\theta_w + u_L\theta_L \tag{2}$$

where u_b is the bubble velocity relative to the vessel and u_L the interstitial liquid velocity relative to the vessel. In turn the bias flux is given by,

$$j_b = j_w - j_f = -u_L\theta_L = -u_L\left(1-\theta_w\right). \tag{3}$$

The bubble slip velocity is the velocity of the bubble relative to the interstitial fluid. That is,

$$V_{slip} = u_b - u_L. \tag{4}$$

The Richardson and Zaki (1954) equation provides a useful basis for describing the bubble velocity, relative to the vessel, under batch conditions (see Appendix A). That is,

$$V_s = V_t \left(1-\theta\right)^n. \tag{5}$$

Here θ is the volume fraction of the dispersed phase. Note that bubble coalescence is assumed to be negligible. The corresponding slip velocity provides a constitutive relationship that is useful here, especially for a bubbly system. That is,

$$V_{slip} = V_t \left(1-\theta\right)^{n-1}. \tag{6}$$

We now combine Equations 1 and 2, insert Equation 4 to replace u_b and then Equation 3 to replace u_L. Equation 5 is then inserted to eliminate the slip velocity, giving,

$$j_g \left(1-\theta_w\right) = V_s \theta_w + \left(j_f - j_w\right)\theta_w. \tag{7}$$

It is noted that the value of V_s in Equation 7 is evaluated at the concentration, θ_w. Dickinson and Galvin (2013) provided the well-known relationship between the gas flux and volume fraction of bubbles in the zone above the level of water injection;

$$\frac{V_{sb}}{j_g} = \frac{1-\theta_b}{\theta_b^{\,2} n} \tag{8}$$

Here the bubble rise velocity, V_{sb}, is evaluated using the corresponding volume fraction of the bubbles, θ_b, above the level of the fluidization water injection. Dickinson and Galvin (2013) then showed the liquid flux, j_f, can be obtained using,

$$\frac{j_f}{j_g} = \frac{(1-\theta_b)}{\theta_b} - \frac{(1-\theta_b)}{\theta_b^{\,2} n}. \tag{9}$$

The above analysis provides a Drift Flux description of the steady state one-dimensional two-phase flow of bubble and fluid components in a conventional system (Wallis, 1969). An example of its application is shown in Figure 4, based on V_t = 15 cm/s and n = 2.5, and a series of example calculations is presented in the Appendix. The bold continuous curve applies to the j_w = 0 case, with two conjugate volume fractions, θ_b and θ_{b1} evident for a given gas flux. The dash curve meeting the bold curve describes the locus of the flooding conditions for wash water fluxes in excess of j_w = 0 cm/s (see Appendix A). As is illustrated in Figure 3A, the upper volume fraction, θ_b, applies to the foam and the lower volume fraction, θ_{b1}, to the dilute bubbly zone. The two thin continuous curves apply to different fluidization wash water flux values distributed down through the foam, j_w = 0.2 and j_w = 2.0 cm/s. Now three conjugate volume fractions exist for a given gas flux and fluidization flux, as shown in Figure 3B. The bubble volume fraction, θ_b, in the foam above the wash water injection junction remains unaffected. Beneath the junction the bubble volume fraction, θ_w, in the concentrated bubbly zone is reduced by the addition of wash water. In turn, the volume fraction, θ_{w1}, in the dilute bubbly zone is increased to above θ_{b1}. Furthermore, as the wash water flux increases, the flooding condition, given by $\theta_b^* = \frac{2}{n+1} \sim 0.57$ for n = 2.5 and j_w = 0 (Wallis, 1969), shifts from the far right to the left, to lower maximum values of j_g. Clearly, with j_g = 4.7 cm/s and j_w = 2.0 cm/s, this study has been conducted at gas fluxes well beyond the flooding limit.

In the present study, however, the system is permitted to expand downwards and into a zone of inclined channels. Here the segregation between the bubbles and the liquid is enhanced, insuring the retention of the gas bubbles in the upper part of the system. Doroodchi et al. (2004) examined this condition for a single component system of solid particles, in which fluidization water was used to cause bed expansion upwards into a single inclined channel.

They showed that the system departs from the usual bed expansion curve defined by the Richardson and Zaki (1954) equation, resulting in finite and significantly greater particle volume fractions, even at superficial velocities much larger than the terminal velocity of the particles. The same applies here, and hence the volume fraction of bubbles is permitted to build towards the level for flooding, and arguably beyond this level.

This increase in volume fraction can be achieved by firstly increasing the tailings rate, and in turn drawing the system of bubbles towards the entrance to the inclined channels, secondly by increasing the fluidization wash water flux, and thirdly by increasing the gas flux. The bed expansion soon comes to a halt due to the increased segregation of the bubbles within the inclined channels, which in turn manifests this increase in the volume fraction of the bubbles to levels much higher than predicted using Drift Flux theory.

In conventional flotation the bubbly zone will generally have a bubble volume fraction less than 0.25 (Finch et al., 2000; Gorain et al., 1995), while in the Reflux Flotation Cell the volume fraction of the "wet" foam/concentrated bubbly zone can rise to more than 0.5, typical of the flooding condition. The zone is characterized by nearly spherical bubbles. This high concentration provides a form of "safety net", insuring the re-capture of any hydrophobic particles dislodged from a rising bubble. Furthermore, due to the absence of a froth zone, coalescence is minimized, and therefore the bubble surface area flux is preserved (Neethling and Cilliers, 2002), and hence particle recovery is maintained.

There is considerable structural change that arises as the concentrated bubbly zone accelerates towards the central outlet on exiting the system, which can lead to coalescence, liquid loss, and reformation of the bubbly flow. It does not follow, however, that these changes lead to a net loss of flotation product, perhaps because of the high concentration of bubbles and rapid increase in the bubble surface flux passing through a decreasing cross-sectional area.

3. Experimental

The experimental Reflux Flotation Cell system used in this study is shown schematically in Figure 1. The feed slurry was pumped to an elevation above the system, and then injected into the downcomer. The downcomer arrangement is shown in Figure 5. The gas flow enters through the top, passing into a 25.4 mm diameter sparger formed from sintered stainless steel. The tubular material was supplied by Mott Pacific, and rated 10 media grade. The sparger tube had a length of 300 mm, and was then attached to a smooth tube 230 mm long of the same diameter, sealed at the top and the bottom. Thus overall an inner tube, 530 mm long was formed, within an outer annulus. This outer annulus was defined by the external tube of external diameter 38.1 mm and inner diameter 35.0 mm. The feed slurry was forced down through the outer annulus, resulting in a high shear rate at the surface of the sparger, ideal for producing air bubbles at the sparger surface, and for promoting efficient collisions between the particles and the air bubbles.

A sleeved sparger based downcomer provides a number of experimental advantages. Firstly, it is possible to independently vary the sparger material, and the gap within the outer annulus, while also varying the volumetric gas and liquid rates. A second advantage of a sleeve and frit downcomer is the ability to control the bubble size independently of the gas flux, and gap size, by controlling the shear generated by the flow of liquid in the annular gap between the sparger surface and sleeve (Kracht et al., 2008). Both the size range and frequency of bubbles leaving such sleeved sparger arrangements have been well modelled (Johnson and Gershey, 1991). A self-aspirating system, as used in the Jameson Cell, while conceptually attractive, and of proven practical advantage, would have provided less independent control over the bubble size for a given shear rate. Note that in this specific study referred to here that independent control was not necessary, but it is needed across the range of experimental studies that are now underway. Finally it is noted that the mean bubble diameter ($d_b = \Sigma d_i^3/\Sigma d_i^2$) was measured to be 1.5 mm, with evidence of some bubbles as small as 0.25 mm, and others up to 2.5 mm. Some coalescence is probable at the relatively low dose of frother deployed.

As noted earlier, the upper free-surface is enclosed by a fluidization distributor (plenum chamber), with a grid of 1.5 mm diameter holes located on four faces of a truncated rectangular pyramid. The holes were evenly spaced from one another, 20 mm apart, with 20 holes on the two larger faces, and 19 on the two adjacent small faces. The fluidization water was fed via a peristaltic pump to the plenum chamber via a four-way manifold. This water contained frothing agent at a concentration equivalent to the feed concentration chosen for this series of experiments. We have not established yet the importance of maintaining the frothing agent at the level applied to the feed water. At this early stage of investigation, however, it makes sense to not compromise the integrity of the gas bubbles unnecessarily by effectively diluting the surfactant concentration around the gas bubbles.

The model feed system was formed using a 50% by mass portion of coal flotation product, which was subjected to wash water, and 50% mass portion of fine silica. Prior to use, the flotation product was wet screened at 260 microns. Once screened, sufficient time was allowed to insure all the fine particles had settled out and were not lost during the decanting of excess water. Table 1 provides a summary of the flotation product used, with the overall material at 10.1 % ash. These data provide a very convenient reference point for assessing the recovery of the coal across the full range of particle size from 0 to 260 microns. The coarser particles have a relatively low fractional ash %, while the finer particles have the higher fractional ash %. Indeed, the 18.2 % ash in the -38 microns particle size range suggests incomplete desliming of the finer gangue material from the original flotation product, which was obtained from a conventional cell that had wash water applied from above the free-surface of the froth. Table 2 shows the mass portion of the fine silica in different size fractions, with more than 98% by mass finer than 38 microns, and the nominal top size less than 63 microns.

Table 3 shows the overall feed, produced when equal mass portions of the flotation product and fine silica are combined. Some variation from one run to the next was obtained. It is evident the cumulative ash % obtained on the overall feed was nearly 60%. This feed was submitted to an external laboratory for analysis using the "Tree Flotation" method. Here the objective is to establish the highest possible cumulative yield by flotation versus the cumulative ash %, by conducting a series of batch separations, using incremental additions of reagent (Brown and Hall, 1999). This method of analysis is widely used to establish the best possible level of separation performance by flotation. While it is true that a density based separation may produce a better result, the gravity separation approach is highly problematic because of the great difficulty of desliming the very finest of particles. So, Tree Flotation analysis provides a boundary of data denoting the best possible flotation achievable. These data were also used in this study to quantify the performance of the Reflux Flotation Cell.

A 9% w/w solids feed slurry, prepared in a 120 litre mixing tank, was pumped up towards the top of the downcomer using a peristaltic pump. The feed tank was regularly topped up during the course of each experiment. Before entering the downcomer, a second pump was used to deliver a MIBC solution to the feed slurry via a T-piece. This reduced the solids content entering the system to 4.5% w/w solids. The experiments were conducted using a MIBC frothing dose of 20 ppm and a diesel dose of 0.5 kg/tonne of coal flotation product. The gas flow to the system was controlled via a Fisher and Porter rotameter.

The tailings discharge was controlled using two pumps. One pump was set at a fixed rate and a second variable speed pump used to provide the finer adjustment. When the wash water rate was increased, it was necessary to increase the liquid tailings rate through the base. If the tailings rate was increased too much, there was a loss of steady discharge in the bubbly flow product. Of course, all of the gas still passed out through the top of the system. It was a straightforward exercise to set a sufficient tailings rate in an experiment. By controlling the tailings rate of discharge, Dickinson and Galvin (2013) found that the liquid overflow rate emerging was very consistent, and tended to increase directly with an increase in the gas flux. Certainly the liquid overflow rate emerging could be maintained to the level obtained in the absence of any wash water. This means that virtually all of the added wash water readily reports as positive bias in the Reflux Flotation Cell, providing efficient desliming.

Once the system had reached steady state, the feed, product, and tailings streams were sampled over timed intervals. Duplicate samples were taken, with typically 1.5 and 3 minutes between the feed and tailings, and product samples respectively. This approach was used to help confirm steady state. Samples were later deslimed at 38 microns, and the dried +38 micron portion sieved using a sieve shaker into several size fractions. It is emphasized that samples were permitted to settle completely in order to ensure the full recovery of all slimes.

The mass % and the ash % (analysed by an outsourced company) of each size fraction were then determined.

The experimental conditions, defined in terms of the fluidization and gas flux values, are plotted in Figure 2. Two series of experiments were conducted. The first involved a level of wash water addition that would be regarded as significant in a conventional system, but relatively low here. The gas flux ranged from low to high, and on to extreme. In this set of experiments the fluidized bed of bubbles was maintained at a distance of 500 mm above the outlet of the downcomer, 170 mm below the fluidization distributor. Thus the concentrated bubbly zone existed well above the system of inclined channels. In the second series of experiments, the fluidization flux was extreme in all cases, while again the gas flux ranged from low to high, and onto extreme. Here, the fluidized bed was drawn into the channels, by increasing the tailings rate, to maintain the overflow liquid flux in proximity to the levels of the first series of experiments. The system of parallel inclined channels positioned beneath the vertical fluidization zone consisted of eight evenly spaced channels, 9.3 mm apart, inclined at 70° to the horizontal. These conditions selected for this study provide a test of performance over a very broad range. They do not denote optimal performance. All fluxes reported were calculated over an area of 0.0072 m^2, based on the cross-sectional area of the Reflux Flotation Cell, less the area occupied by the downcomer.

4. Results and Discussion

Figure 6 shows the combustible recoveries achieved using the Reflux Flotation Cell versus the gas flux obtained using the relatively low wash water flux of 0.2 cm/s, and with the fluidized bed of bubbles maintained above the downcomer outlet. Thus in this case the concentrated bubbly zone existed well above the system of inclined channels. The corresponding product ash % values are shown in Figure 7. It is evident that very high combustible recoveries were achieved, with the recovery increasing directly with the gas flux. The corresponding product ash % values were relatively low when the gas flux was low, and remained remarkably low at the high gas flux of 2.6 cm/s, however, the product ash % increased significantly at the extreme gas flux level of 4.7 cm/s. It should be noted that the mean feed ash used was 58% and hence the performance across the full gas flux range was very high. Moreover, the original model feed ash was 10.1%, and hence the Reflux Flotation Cell produced a significant improvement in the product quality while delivering almost full combustible recovery. Of course at the extreme gas flux of 4.7 cm/s there was clear evidence of additional silica entrainment into the product.

Table 4A provides a detailed summary of the run performed at the high gas flux of 2.6 cm/s and wash water flux of 0.2 cm/s, showing the mass % and ash % for each size fraction, along with the cumulative values. Table 4B provides the corresponding data on the yield and combustible recovery. It is evident that in the relatively coarse size fractions the portion of material reporting to the tailings stream is very low, and the corresponding ash % relatively high. Thus the only losses in these size fractions are particles that should not have been present in the original flotation product. In the finer size fractions there is clear evidence of improvement in the product quality over the original flotation product shown in Table 1, with much lower fractional ash levels obtained. In the tailings stream, the recovery of the fine silica is very clear, with the % mass and ash level of the finest size fraction at 95.4% and 99% respectively. Previously, using a hydrophilic silica-only model feed with a slightly higher feed pulp density of 6.5% solids, Dickinson and Galvin (2013) demonstrated the rejection of 98.4% silica using a similar level of wash water and using much finer sized bubbles, with a mean bubble diameter of 340 microns. Hence the Reflux Flotation Cell demonstrates a robust ability to reject entrainment when subjected to a variable content of hydrophilic particles.

Table 4B shows the very high combustible recoveries obtained at each size fraction, up to 99%, with the overall recovery at 98%. Thus at this relatively low wash water flux, but very high gas flux, nearly complete combustible recovery was achieved, along with a high product quality.

Included in Figures 6 and 7 are the separations achieved when an extreme wash water flux of nominally 2.0 cm/s was used in the Reflux Flotation Cell. In this series of experiments the fluidized bed was expanded into the inclined channel, typically to a channel depth of 120 mm, in order to maintain a reasonable liquid flux reporting to the overflow. The combustible recoveries are clearly lower than obtained for the relatively low wash water fluxes, at about 75%. This reduction in recovery might be of concern if the losses were indiscriminate, however, the product ash levels produced are significantly lower at about 5%, well below the original flotation product ash of 10.1%, and below the level obtained using the Reflux Flotation Cell at the relatively low wash water flux. Interestingly, at the extreme gas flux level of 4.7 cm/s the product ash is 6%, well below the ash % obtained in the previous series when a relatively low wash water flux was used. Clearly, by drawing the concentrated bubbly zone into the inclined channels and preventing excess liquid to flow to the overflow, the extreme wash water flux was able to prevent the excess slimes entrainment that arises when an extreme gas flux is used without the enhanced segregation of inclined channels.

Tables 5A and 5B provide the detailed data on the separation performance for each size fraction for a gas flux of 0.5 cm/s and extremely high wash water flux of 2.1 cm/s. The fractional ash values in the coarser size fractions are less than 3%, while the ash levels of the finer particles are higher at about 6%, combining to give a product ash of 4%. Note that the -38 μm size fraction in the feed was reduced from 88.5% ash to a product ash of 5.7%. In the tailings, the particles have relatively moderate ash % levels hence the combustible recoveries are lower than obtained previously.

Figures 8 and 9 show the combustible recovery and product ash versus the fluidization water flux to gas flux ratio, respectively, for low and extreme levels of applied wash water. In each figure the combined data demonstrates a rapid decline in the value of combustible recovery, and product ash, with increasing fluidization flux to gas flux ratio, then trending off to a near asymptotic value. This ratio describes the degree of interfacial washing and hence product cleaning. Particles that have a lower contact angle will tend to be the least hydrophobic (Jameson, 2012). In coal preparation, these particles are also denser, and hence contain more mineral matter, and thus have the higher ash %. Thus it seems the high counter-current hydrodynamic conditions produced circumstances that stripped weakly hydrophobic particles from the bubbles. Clearly the Reflux Flotation Cell withstood extreme wash water fluxes, delivering very high selectivity, with only the lowest ash particles remaining attached to the bubbly flow product.

The liquid flux reporting to the product overflow increases directly with the gas flux, a result predicted using Drift Flux theory (Dickinson et al., 2010). Figure 10 shows the liquid product flux obtained in this study, for both the relatively low and extreme fluidization fluxes. While the extreme level of fluidization wash water produced the higher liquid flux reporting to product, the additional liquid was relatively small compared to the ten-fold increase in the fluidization flux. However, as is demonstrated in Figure 11, the combined effect of a marginally greater overflow liquid flux, but lower ash combustible product, did result in a lowering of the product pulp density when fluidizing at an extreme wash water flux. Arguably, since only a small portion of the 1 m channels was occupied by the fluidized bed, the tailings rate could have been further increased to decrease the overflow liquid flux. This would have aided the desliming, and dewatering, of the product overflow.

There were two additional conditions that were examined using the extreme wash water fluidization flux of 2.0 cm/s. The results obtained are included in Figures 12 and 13. In the first of these additional experiments a relatively low gas flux of 0.5 cm/s was used. With the extreme wash water fluidization flux, the concentrated bubbly zone was normally extended downwards and into the inclined channel zone. However, in this experiment the tailings rate was deliberately reduced, resulting in the concentrated bubbly zone failing to interact with the inclined channels. Hence the concentrated bubbly zone rose and was positioned to a level above the outlet of the downcomer. This change resulted in a three-fold increase in the liquid flux reporting to the overflow, with a clear increase in the product ash, from 4.0% to 6.4%. However, a significant reduction in combustible recovery followed, from 74.7% to 66.4%, due to an increasing loss of the coarse particles. For instance, the -260+212 μm fractional recovery decreased from 65.0% to 4.9%. This result shows the functional importance of extending the fluidized bubbly zone downwards towards the inclined channels. The high concentration of bubbles below the downcomer provides a crucial “safety net” that supports the recovery of the coarser particles under these extreme hydrodynamic conditions.

In the second of these additional experiments the extremely high gas flux of 4.7 cm/s was used. Again the fluidization wash water flux was extreme at 2.0 cm/s. This time the reduction in the tailings rate resulted in a two-fold increase in the liquid flux reporting to the product. The key difference in this experiment is that the concentrated bubbly zone still remained adjacent to the inclined channel zone. In other words, the “safety net” offered by the high concentration of bubbles was still in place below the downcomer exit, though technically the inclined channels were not engaged by the concentrated bubbly zone. In this run the combustible recovery was found to in fact increase from 76.5% to 94.4%, while the product ash only increased from 6.2% to 8.6%. Therefore, these conditions delivered one of the best separations, in terms of high recovery and satisfactory product ash. For example, at the lower wash water flux of 0.2 cm/s the recovery was only slightly higher at 97.3%, while the product ash was significantly higher at 14.2%. The importance of the concentrated bubbly zone safety net is well supported by these results. These data also appear to be in agreement with recent claims that the recovery of coarser particles is related to the hydrodynamic condition in a chemically constant flotation cell, independent of the particle size for a given fractional surface liberation (Jameson, 2012). The issue of recovering much coarser particles will be the subject of a further study.

It is worth considering the solids concentration of the overflow product, especially in the context of both the low and the extreme fluidization wash water fluxes. The overflow pulp density is shown as a function of the gas flux in Figure 11. Clearly, where there exists the need to meet a given pulp density of, for example, 10% solids by weight, there is a clear basis for limiting the gas and wash water fluxes. Another useful representation is the ratio of the fluidization wash water flux to the liquid overflow flux (Atkinson et al., 1993), hereby referred to as the *fluidization to overflow ratio*. Figure 12 shows the bias flux plotted versus the fluidization to overflow ratio. The region within the dashed rectangle denotes the operating regime of conventional flotation (Atkinson et al., 1993; Yianatos et al., 1987). Clearly, the operating regime of the Reflux Flotation Cell extends well beyond the usual levels. What is most apparent is that a very broad range of bias is achievable, depending on the degree of desliming that is required, and that the limit on the bias flux is achieved within a fluidization to overflow ratio of 10.

In order to place this work into a more reliable context, the model feed system was sent to an independent laboratory with a request for a Tree Flotation Analysis. The overall Tree Flotation result is shown in Figure 13, along with the data produced using the Reflux Flotation Cell, at a relatively low and extreme fluidization flux. It is evident that the separation performance is to the right of the Tree Curve when the fluidization flux is at the relatively low level of order 0.2 cm/s. Moreover, the steep nature of the curve helps to account for the range of combustible recoveries obtained. What is especially interesting is that a few results, obtained using the extreme fluidization flux, lie to the left of the Tree Curve. These three points correspond to a fluidization to overflow ratio greater than 11 in Figure 12. Some would argue that this separation should not be possible, certainly under continuous steady state conditions, using a single reagent dose and single stage separation. However, it should be pointed out that the hydrodynamic circumstances deployed in this study are very unusual. The fluidization wash water flux used was an order of magnitude higher than levels normally deployed in practice. The system of inclined channels produced well-defined, and intense, conditions for stripping the lower contact angle particles from the bubbles. The high fluidization rate would normally produce significant bed expansion, and hence losses of bubbles to tailings, however, as noted earlier, the inclined channels prevent this loss, resulting in a higher level of gas hold up. It is the view of the authors that these unique conditions lead to the remarkably low ash % values, below that achieved using the Tree Flotation method.

5. Conclusions

This study demonstrated that the Reflux Flotation Cell is a robust system, capable of being operated successfully at extreme levels in the values of the fluidizing wash water and gas fluxes. A wash water flux of up to 2.0 cm/s can be accommodated, while a gas flux of up to 4.7 cm/s can be applied, corresponding to a bubble surface flux of 188 $m^2/m^2.s$ based on a mean bubble diameter, d_b, of 1.5 mm. Arguably, there is no flotation device in existence, operated solely in the gravitational field, which can withstand the conditions described in this paper. Optimal operation, which will depend on the specific objectives, should be achievable well within this vast operating regime.

The study demonstrated that a full combustible recovery of fine coal can be achieved, while achieving the full rejection of ultrafine hydrophilic particles of silica. The results were in good agreement with those obtained using the Tree Flotation method. Moreover, the separation performance achieved was consistent across the full particle size range examined, from 0 to 260 microns. At an extreme fluidization flux selective stripping of coal particles from the bubble surface was achieved, resulting in a product ash well below that obtained using the Tree Flotation method.

The novel flotation system clearly offers remarkable performance in desliming due to the strong counter-current washing process and strong positive bias. Future work will focus on the improved kinetics expected as a result of the high gas fluxes. The high volume fraction of bubbles that develop within the concentrated bubbly zone at the high gas fluxes deployed provides a form of “safety net”, hence particles that detach should readily re-attach. Thus future work will also focus on the flotation of particles across a much broader size range.

6. Disclosure Statement

The University of Newcastle holds international patents and patent applications on the Reflux Classifier and related technologies and has a Research and Development Agreement with FLSmidth Ludowici to develop these technologies.

7. Acknowledgements

The support of the Australian Coal Association Research Program and the Australian Research Council is appreciated and acknowledged.

8. References

Atkinson, B.W., Conway, C.J., Jameson, G.J., 1993. Fundamentals of Jameson Cell operation including size - yield response, VI Australian Coal Preparation Conference, Mackay.

Boycott, A.E., 1920. Sedimentation of blood corpuscles. Nature 104, 532.

Brown, D.W., Hall, S.T., 1999. Froth flotation: preparation of a laboratory standard. Fuel 78, 1621-1629

Dickinson, J.E., Galvin, K.P., 2013. Fluidized Bed Desliming in Fine Particle Flotation - Part I. Chemical Engineering Science, Accepted.

Dickinson, J.E., Laskovski, D., Stevenson, P., Galvin, K.P., 2010. Enhanced foam drainage using parallel inclined channels in a single-stage foam fractionation column. Chemical Engineering Science 65, 2481-2490.

Doroodchi, E., Fletcher, D.F., Galvin, K.P., 2004. Influence of inclined plates on the expansion behaviour of particulate suspensions in a liquid fluidised bed. Chemical Engineering Science 59, 19-25.

Finch, J.A., Xiao, J., Hardie, C., Gomez, C.O., 2000. Gas dispersion properties: bubble surface area flux and gas holdup. Minerals Engineering 13, 365-372.

Fuerstenau, M.C., Jameson, G.J., Yoon, R.H., 2007. Froth Flotation: A Century of Innovation. SME, pp. 641, 685, 734.

Galvin, K.P., Zhou, J., Dickinson, J.E., Ramadhani, H., 2012. Desliming of dense minerals in fluidized beds. Minerals Engineering 39, 9-18.

Galvin, K.P., Zhou, J., Walton, K., 2010. Application of closely spaced inclined channels in gravity separation of fine particles. Minerals Engineering 23, 326-338.

George, P., Nguyen, A.V., Jameson, G.J., 2004. Assessment of true flotation and entrainment in the flotation of submicron particles by fine bubbles. Minerals Engineering 17, 847-853.

Goel, S., Jameson, G.J., 2012. Detachment of particles from bubbles in an agitated vessel. Minerals Engineering 36–38, 324-330.

Gorain, B.K., Franzidis, J.P., Manlapig, E.V., 1995. Studies on impeller type, impeller speed and air flow rate in an industrial scale flotation cell part 2: Effect on gas holdup. Minerals Engineering 8, 1557-1570.

Jameson, G.J., 2012. The effect of surface liberation and particle size on flotation rate constants. Minerals Engineering 36–38, 132-137.

Johnson, B.D., Gershey, R.M., 1991. Bubble formation at a cylindrical frit surface in a shear field. Chemical Engineering Science 46, 2753-2756.

Kracht, W., Gomez, C.O., Finch, J.A., 2008. Controlling bubble size using a frit and sleeve sparger. Minerals Engineering 21, 660-663.

Lorenceau, E., Louvet, N., Rouyer, F., Pitois, O., 2009. Permeability of aqueous foams. European Physical Journal E 28, 293-304.

Massinaei, M., Kolahdoozan, M., Noaparast, M., Oliazadeh, M., Yianatos, J., Shamsadini, R., Yarahmadi, M., 2009. Hydrodynamic and kinetic characterization of industrial columns in rougher circuit. Minerals Engineering 22, 357-365.

Neethling, S.J., Cilliers, J.J., 2001. Simulation of the effect of froth washing on flotation performance. Chemical Engineering Science 56, 6303-6311.

Neethling, S.J., Cilliers, J.J., 2002. Solids motion in flowing froths. Chemical Engineering Science 57, 607-615.

Richardson, J.F., Zaki, W.N., 1954. Sedimentation and fluidisation: Part I. Trans IChemE 32, 34-53.

Rouyer, F., Pitois, O., Lorenceau, E., Louvet, N., 2010. Permeability of a bubble assembly: From the very dry to the wet limit. Physics of Fluids 22, 1-5.

Wallis, G.B., 1969. One-dimensional two-phase flow. McGraw-Hill, New York.

Yianatos, J.B., Finch, J.A., Laplante, A.R., 1987. Cleaning action in column flotation froths. Trans. Inst. Min. Metall. C, C199-C205.

Zang, P., Snow, R., Miller, J., Kohmuench, J., 2004. Improving Phosphate Flotation with New Chemistry, Smart Flowsheet, and Novel Equipment, SME Annual Meeting, Feb 23-25, Denver Colarado, Preprint 04-72

Appendix A

In this Appendix the conditions associated with the zone below the elevation of water injection is examined. Two zones exist below the injection point, firstly, the "wet" foam zone, referred to as a concentrated bubbly zone, directly beneath the injection point, and secondly, the dilute bubbly zone below the concentrated bubbly zone. A flux balance is used to obtain the bias flux and the volume fraction of bubbles in each zone. The basic approach involves firstly describing the foam zone above the elevation of the wash water injection, utilizing Drift Flux theory. In this example an implicit iterative approach is used to obtain the gas flux, j_g, for a given θ_b. The values used in this example are: bubble terminal velocity, V_t = 15 cm/s, n = 2.5, and θ_b = 0.88. Figure A1 shows the Drift Flux curve for this analysis.

The gas flux imposed to obtain θ_b = 0.88 in the foam zone is found through trial and error. Hence we guess that j_g = 1.207 cm/s. We can now calculate the bubble velocity relative to the vessel in the absence of fluidization by using Equation 8. That is,

$$\frac{V_{sb}}{j_g} = \frac{1-\theta_b}{\theta_b^{\,2} n},$$

$$V_{sb} = 1.207\left(\frac{1-0.88}{0.88^2 \times 2.5}\right) = 0.07483\,\mathrm{cm/s}.$$

This result is consistent with the direct calculation of Equation 5. That is,

$$V_{sb} = V_t\left(1-\theta_b\right)^n = 15\left(1-0.88\right)^{2.5} = 0.07483\,\mathrm{cm/s}.$$

Hence the gas flux required to obtain a bubble volume fraction of θ_b = 0.88 in the foam zone is j_g = 1.207 cm/s. With the gas flux established, we can now determine the liquid flux in the upper zone by using Equation 9. That is,

$$\frac{j_f}{j_g} = \frac{(1-\theta_b)}{\theta_b} - \frac{\left(1-\theta_b\right)}{\theta_b^{\,2} n},$$

$$j_f = 1.207\frac{(1-0.88)}{0.88} - 1.207\frac{(1-0.88)}{0.88^2 \times 2.5} = 0.08979\,\text{cm/s.}$$

In the lower concentrated bubbly zone, the wash water flux is set at 2.0 cm/s. Then the bias flux is,

$j_b = j_w - j_f = 2.0 - 0.08979 = 1.910\,\text{cm/s}$.

The flux balance applicable to the concentrated bubbly zone below the level of wash water injection is given by Equation 7. That is,

$j_g(1-\theta_w) = V_s\theta_w + (j_f - j_w)\theta_w$.

Again we need to solve the problem through trial and error. Thus we guess that $\theta_w = 0.4478$. The left hand-side of the flux balance is,

$j_g(1-\theta_w) = 1.207(1-0.4478) = 0.6666$ cm/s.

It follows that the bubble velocity under batch conditions is,

$V_s = V_t(1-\theta_w)^n = 15(1-0.4478)^{2.5} = 3.399\;\text{cm/s}$.

It is noted that under batch conditions there is no net flux through the system. At the end of this Appendix this condition is also shown to apply to the bubble velocity relative to the net flux passing through the system. Thus the right hand side is,

$V_s\theta_w + (j_f - j_w)\theta_w = 3.399 \times 0.4478 + (0.08979 - 2.0)0.4478 = 0.6666$ cm/s.

Hence, as the left and right hand-sides are equal, the correct volume fraction in the concentrated bubbly zone is 0.4478.

To calculate the conjugate bubble volume fraction, θ_{w1}, in the dilute bubbly zone, the above flux calculations involving Equation 7 are repeated, however, this time we guess a lower value of $\theta_{w1} = 0.1175$. The left hand-side of the flux balance is,

$j_g(1-\theta_{w1}) = 1.207(1-0.1175) = 1.065$ cm/s.

The bubble velocity under batch conditions is,

$V_s = V_t\left(1-\theta_{w1}\right)^n = 15\left(1-0.1175\right)^{2.5} = 10.97\ \text{ cm/s}$.

Thus the right hand side is,

$V_s\theta_{w1} + \left(j_f - j_w\right)\theta_{w1} = 10.97\times 0.1175 + \left(0.08979 - 2.0\right)0.1175 = 1.065\ \text{cm/s}$.

Hence, as the left and right hand-sides are equal, the correct volume fraction in the dilute bubbly zone is 0.1175 when j_w = 2.0 cm/s.

For the case involving j_g = 1.207 cm/s and j_w = 0 cm/s, the initial analysis in the Appendix shows the volume fraction of the foam is θ_b = 0.88 and j_f = 0.08979 cm/s. To determine the conjugate volume fraction of the bubbles in the dilute bubbly zone, θ_{b1}, it is necessary to repeat the method used to calculate both θ_w and θ_{w1} while using j_w = 0 cm/s. In this example θ_{b1} = 0.09237.

Equation 8, solved using $\theta_b < \dfrac{2}{n+1}$, provides the dash curve shown in Figure 4, which is the locus of the flooding conditions produced using different values of j_w.

It is worth examining the flux contributions of the concentrated bubbly zone. The relevant slip velocity of the bubbles is,

$V_{slip} = V_t\left(1-\theta_w\right)^{n-1} = 15\left(1-0.4478\right)^{2.5-1} = 6.155\ \text{ cm/s}$.

The bias flux is,

$j_b = j_w - j_f = -u_L\theta_L = -u_L(1-\theta_w)$.

Thus, the interstitial liquid velocity is,

$$u_L = -\frac{j_b}{1-\theta_w} = -\frac{1.910}{1-0.4478} = -3.459\,\text{cm/s}.$$

The bubble velocity can be determined using,

$V_{slip} = u_b - u_L$.

Hence, the bubble velocity relative to the vessel is,

$u_b = 6.155 - 3.459 = 2.696$ cm/s.

The bubble flux, which equals the gas flux, is $u_b\theta_w = 2.6696 \times 0.4478 = 1.207$ cm / s.

The interstitial liquid flux is $u_L\theta_L = -3.459(1 - 0.4478) = -1.910$ cm / s .

The total flux is $u_b\theta_w + u_L\theta_L = 1.207 - 1.910 = -0.7030$ cm/s.

The total upwards flux of bubbles and liquid is $j_g - j_b = 1.207 - 1.910 = -0.7030$ cm/s.

Combining the bubble velocity, u_b, relative to the vessel, with the total flux through the system, gives the batch settling velocity of the bubbles. That is,

$V_s = u_b - \psi_T = 2.696 + 0.7030 = 3.399$ cm / s .

As already noted, the batch settling velocity, V_s, provides the bubble velocity relative to the vessel for a system that involves no net flux through the system.

List of Tables

Table 1: Original flotation product, showing fractional and cumulative mass and ash % values.

Size Range (µm)	Mass (%)	Cumulative Mass (%)	Ash (%)	Cumulative Ash (%)
-260+212	11.9	11.9	6.6	6.6
-212+150	22.4	34.3	7.0	6.9
-150+90	27.9	62.1	8.0	7.4
-90+63	13.2	75.3	11.0	8.0
-63+38	8.1	83.5	13.5	8.5
-38+0	16.5	100.0	18.2	10.1

Table 2: Size distribution of the Sibelco 400G silica flour, used in the model feed. About 25.3% of the silica was below 10 microns.

Size Range (μm)	Mass (%)	Cumulative Mass (%)
-63+45	0.3	0.3
-45+38	1.4	1.8
-38+0	98.2	100.0

Table 3: Model flotation feed formed from original flotation product and silica flour on an equal mass % basis.

Size Range (μm)	Mass (%)	Cumulative Mass (%)	Ash (%)	Cumulative Ash (%)
-260+212	4.6	4.6	6.7	6.7
-212+150	11.5	16.1	7.7	7.4
-150+90	13.8	29.9	9.1	8.2
-90+63	6.4	36.2	13.6	9.1
-63+45	3.2	39.5	29.6	10.8
-45+38	2.4	41.9	52.1	13.2
-38+0	58.1	100.0	87.7	56.5

Table 4A: Separation achieved for a very high gas flux of 2.6 cm/s.

Size Range (µm)	MODEL FEED				OVERFLOW (Product)				UNDERFLOW (Reject)			
	Mass (%)	Cumulative Mass (%)	Ash (%)	Cumulative Ash (%)	Mass (%)	Cumulative Mass (%)	Ash (%)	Cumulative Ash (%)	Mass (%)	Cumulative Mass (%)	Ash (%)	Cumulative Ash (%)
-260+212	4.6	4.6	6.7	6.7	10.4	10.4	6.0	6.0	0.4	0.4	70.8	70.8
-212+150	11.5	16.1	7.7	7.4	20.8	31.2	5.9	5.9	0.6	0.9	77.2	74.6
-150+90	13.8	29.9	9.1	8.2	29.4	60.6	6.8	6.4	0.7	1.6	82.0	77.8
-90+63	6.4	36.2	13.6	9.1	12.7	73.3	8.8	6.8	0.5	2.1	84.4	79.3
-63+45	3.2	39.5	29.6	10.8	6.8	80.1	10.7	7.1	0.8	3.0	95.5	83.9
-45+38	2.4	41.9	52.1	13.2	4.1	84.2	12.1	7.4	1.6	4.6	98.2	89.0
-38+0	58.1	100.0	87.7	56.5	15.8	100.0	12.3	8.1	95.4	100.0	99.0	98.5

Table 4B: Recoveries for a very high gas flux of 2.6 cm/s.

Size Range (µm)	PERFORMANCE			
	Yield (%)	Cumulative Yield (%)	Combustible Recovery (%)	Cumulative Combustible Recovery (%)
-260+212	98.9	98.9	99.7	99.7
-212+150	97.5	97.8	99.4	99.4
-150+90	96.9	97.4	99.4	99.4

-90+63	93.7	96.7	98.9	99.3
-63+45	77.7	95.2	98.6	99.1
-45+38	53.5	92.8	98.3	99.1
-38+0	13.0	46.5	92.9	98.2

Table 5A: Separation achieved for a very high wash water flux of 2.1 cm/s.

Size Range (µm)	MODEL FEED				OVERFLOW (Product)				UNDERFLOW (Reject)			
	Mass (%)	Cumulative Mass (%)	Ash (%)	Cumulative Ash (%)	Mass (%)	Cumulative Mass (%)	Ash (%)	Cumulative Ash (%)	Mass (%)	Cumulative Mass (%)	Ash (%)	Cumulative Ash (%)
-260+212	4.8	4.8	6.9	6.9	8.6	8.6	2.8	2.8	1.6	1.6	13.7	13.7
-212+150	8.5	13.3	7.5	7.3	20.2	28.8	2.9	2.9	3.5	5.1	14.0	13.9
-150+90	12.9	26.2	8.4	7.8	35.3	64.0	3.7	3.3	4.6	9.7	18.1	15.9
-90+63	6.1	32.3	12.7	8.8	13.7	77.7	4.5	3.5	2.1	11.9	28.5	18.1
-63+45	3.2	35.4	31.5	10.8	6.6	84.4	5.4	3.7	1.5	13.4	56.6	22.6
-45+38	2.2	37.6	56.0	13.4	4.4	88.7	5.9	3.8	1.9	15.3	79.6	29.5
-38+0	62.4	100.0	88.5	60.2	11.3	100.0	5.7	4.0	84.7	100.0	95.5	85.4

Table 5B: Recoveries for a very high wash water flux of 2.1 cm/s.

Size Range (μm)	PERFORMANCE			
	Yield (%)	Cumulative Yield (%)	Combustible Recovery (%)	Cumulative Combustible Recovery (%)
-260+212	62.4	62.4	65.1	65.1
-212+150	58.6	60.0	61.5	62.8
-150+90	67.4	64.1	70.8	67.3
-90+63	65.8	64.3	72.0	67.9
-63+45	49.0	62.4	67.7	67.3
-45+38	32.0	62.6	68.5	69.6
-38+0	7.8	30.9	63.9	74.7

- Flotation product from a model coal feed is deslimed using a fluidization approach
- Extreme gas and wash water fluxes were achieved, far beyond conventional values
- Full combustible recovery and mineral rejection were obtained
- Selective stripping of coal achieved beneficiation beyond the Tree Flotation method

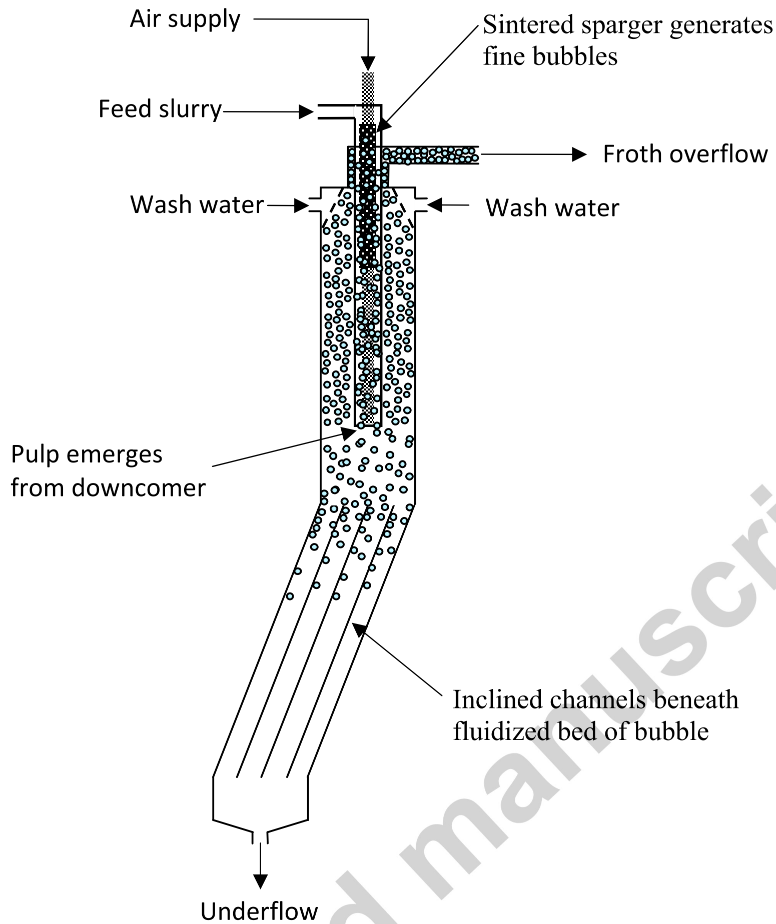

Figure 1: Schematic representation of the Reflux Flotation Cell used in the study. The upper vertical and lower, inclined, sections were both 1 m in length. The channels were inclined to an angle of 70° to the horizontal.

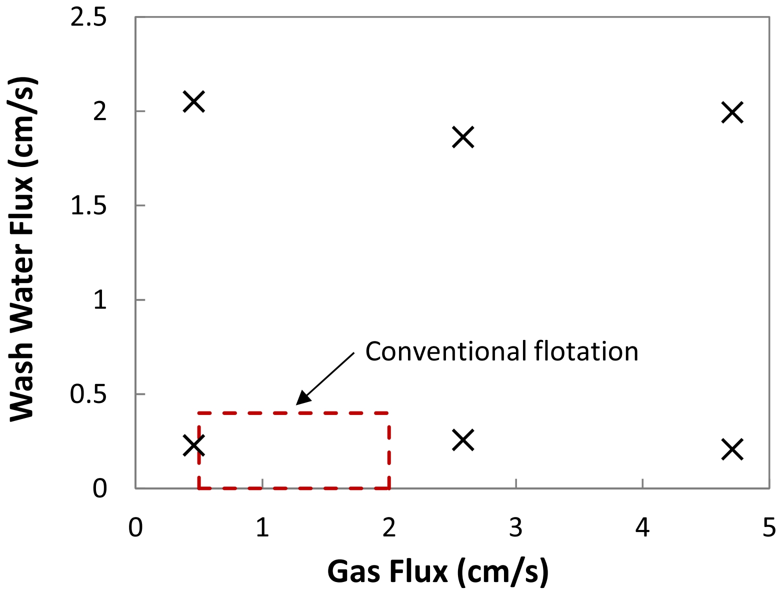

Figure 2: Wash water flux versus gas flux regime investigated in this study is denoted by the cross symbols. This zone is vast compared to that used in conventional flotation.

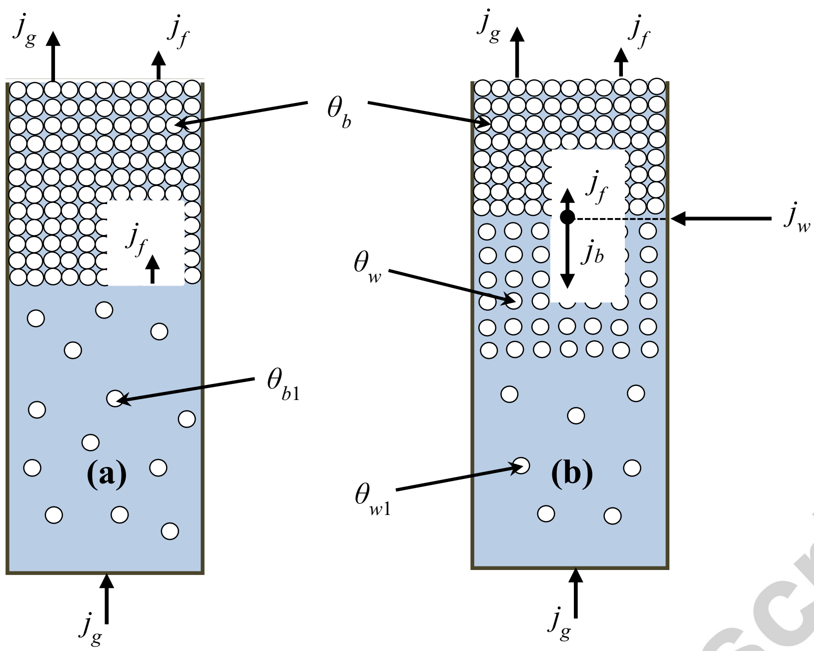

Figure 3: Schematic representation of (A) conventional flotation without wash water addition, and (B) flotation with wash water injected into the foam zone at the junction that defines the upwards liquid flux, wash water flux, and bias flux.

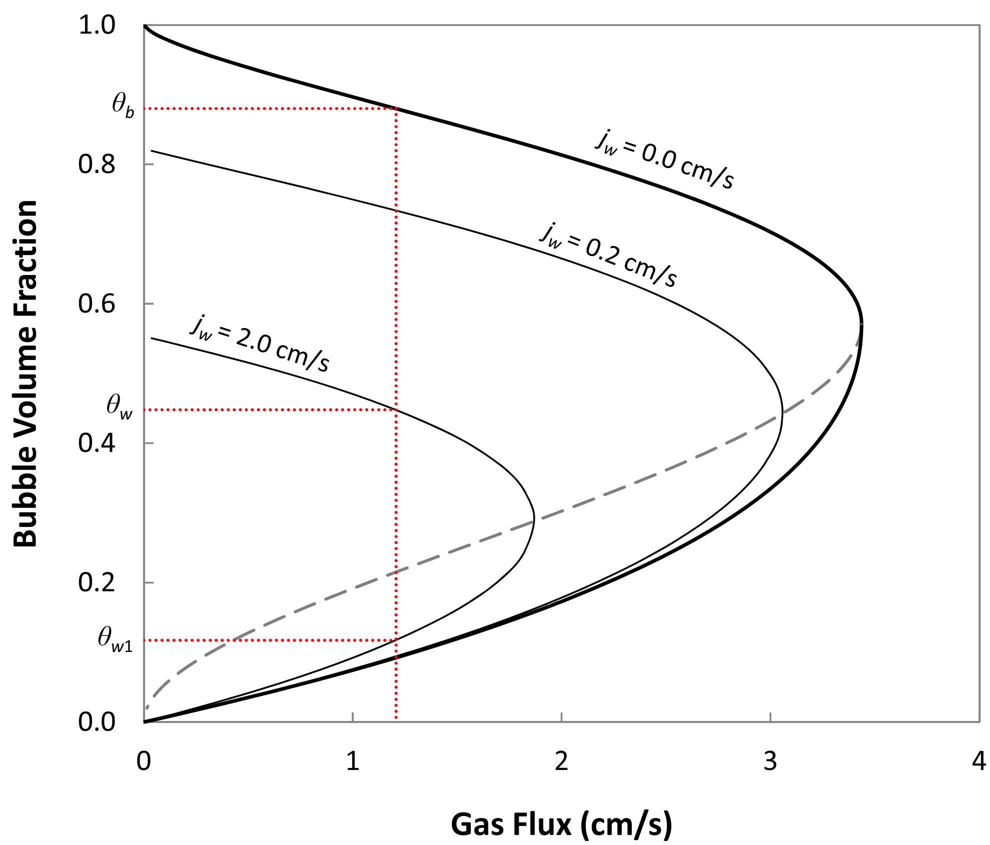

Figure 4: Drift Flux calculations showing the bubble volume fraction as a function of the imposed gas flux. The bubble terminal velocity, V_t = 15 cm/s, and the hindered settling exponent is n = 2.5. The bold continuous curve applies to the j_w = 0 case, with two conjugate volume fractions evident for a given gas flux. The upper volume fraction applies to the foam and the lower volume fraction to the dilute bubbly zone. The dashed curve departing from the bold curve describes the locus of the flooding condition for j_w > 0 cm/s. The thin continuous curves apply to different wash water flux values distributed down through the foam, j_w = 0.2 and j_w = 2.0 cm/s. In each case three conjugate volume fractions are formed. An example calculation for the conjugate set, θ_b, θ_w and θ_{w1} is given in the Appendix.

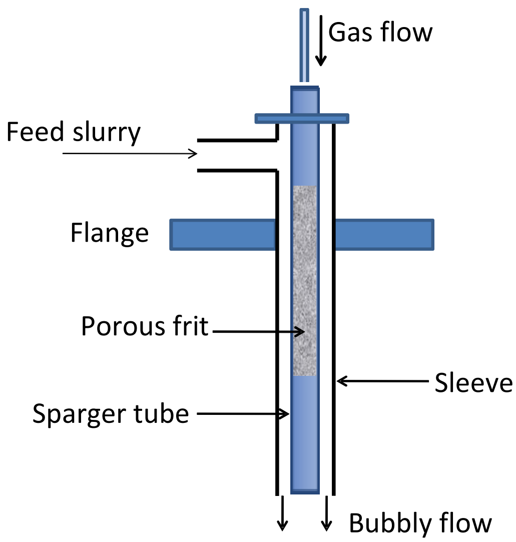

Figure 5: Schematic representation of the downcomer arrangement used for contacting the feed slurry and gas bubbles.

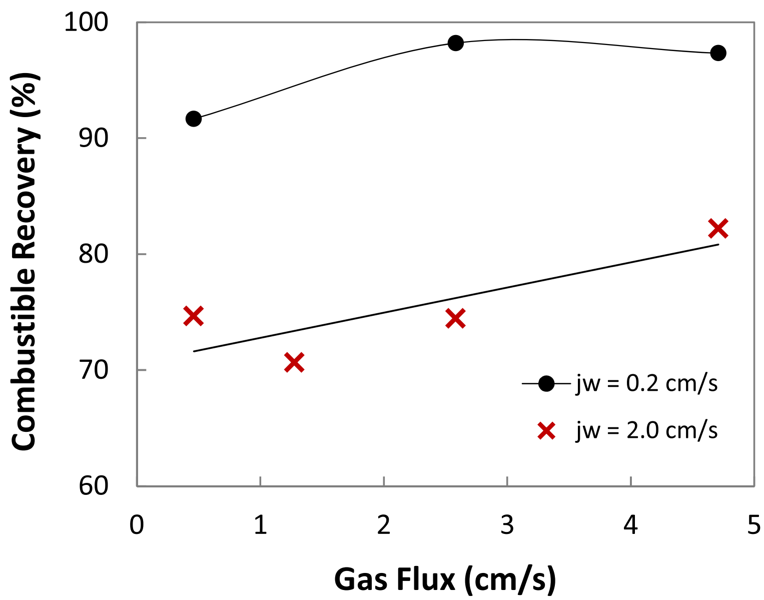

Figure 6: Combustible recovery versus the gas flux. Two series of experiments are shown using firstly, a relatively low wash water flux of 0.2 cm/s and secondly, an extremely high wash water flux of 2.0 cm/s.

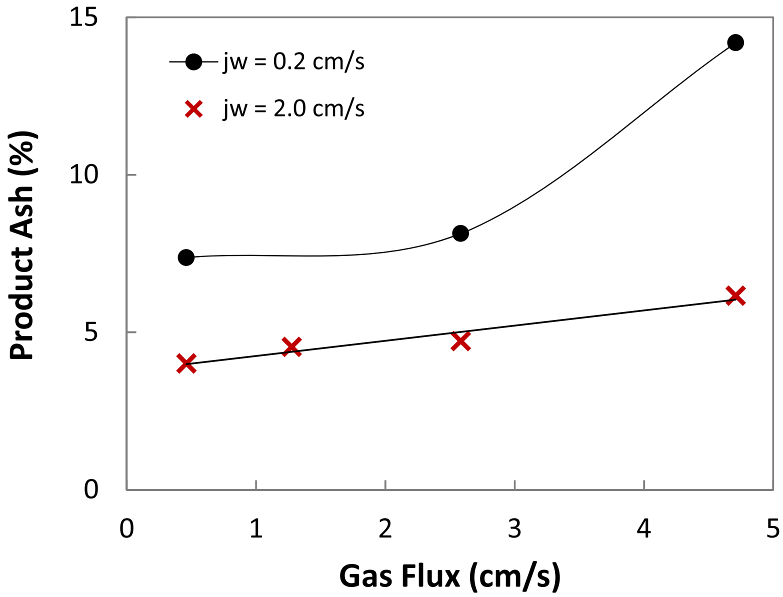

Figure 7: Product ash % versus the gas flux. Two series of experiments are shown using firstly, a relatively low wash water flux of 0.2 cm/s and secondly, an extremely high wash water flux of 2.0 cm/s.

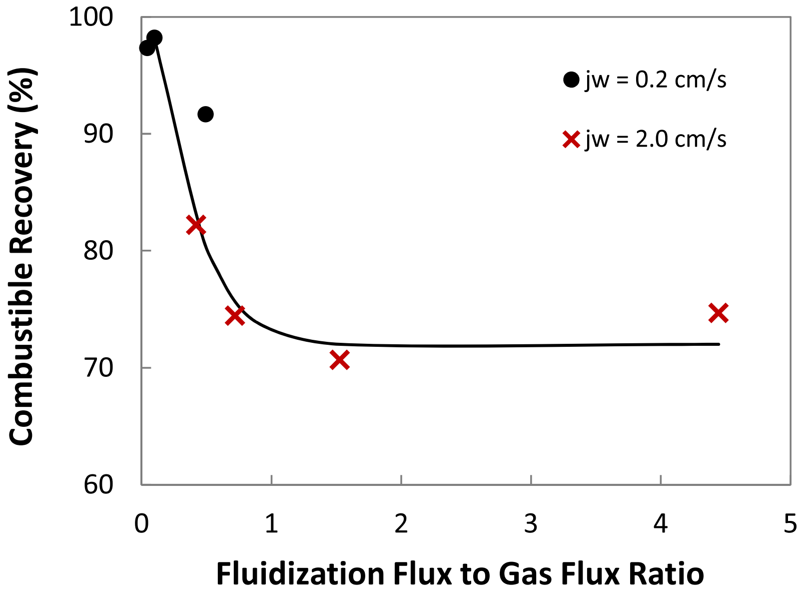

Figure 8: Combustible recovery versus the fluidization flux to gas flux ratio.

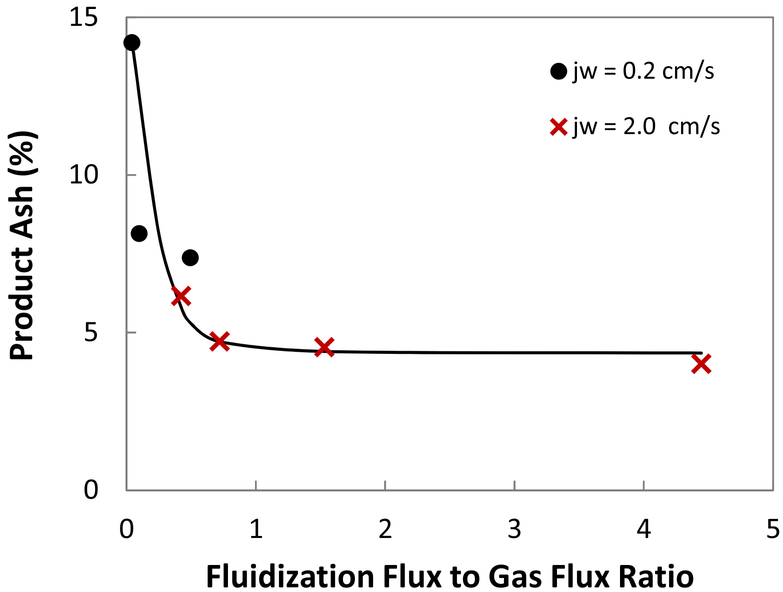

Figure 9: Product ash % versus the fluidization flux to gas flux ratio.

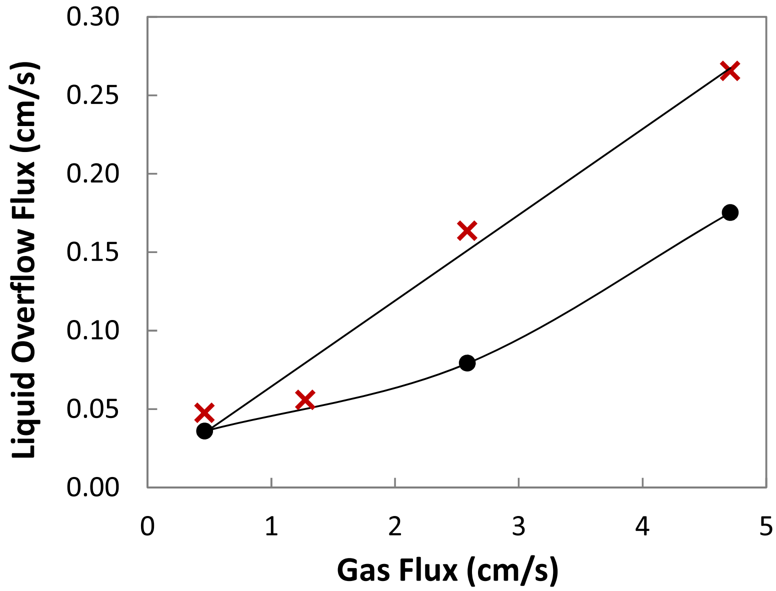

Figure 10: Product liquid flux versus the gas flux. The circles denote the relatively low wash water flux and the crosses the extreme wash water flux.

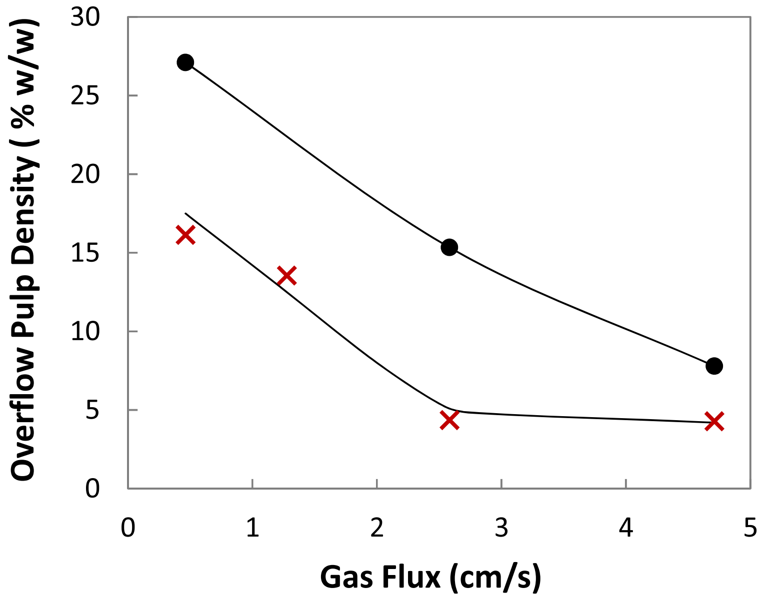

Figure 11: Pulp density of the product overflow versus the gas flux. The circles denote the relatively low wash water flux and the crosses the extreme wash water flux.

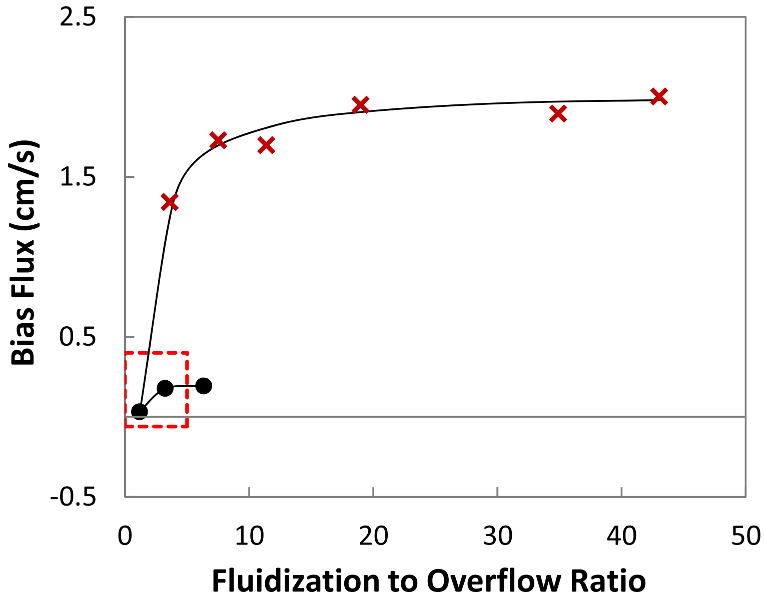

Figure 12: Bias flux versus the fluidization flux to overflow liquid flux ratio. The circles denote the relatively low wash water flux and the crosses the extreme wash water flux. The rectangle encloses the typical operating range used in conventional flotation.

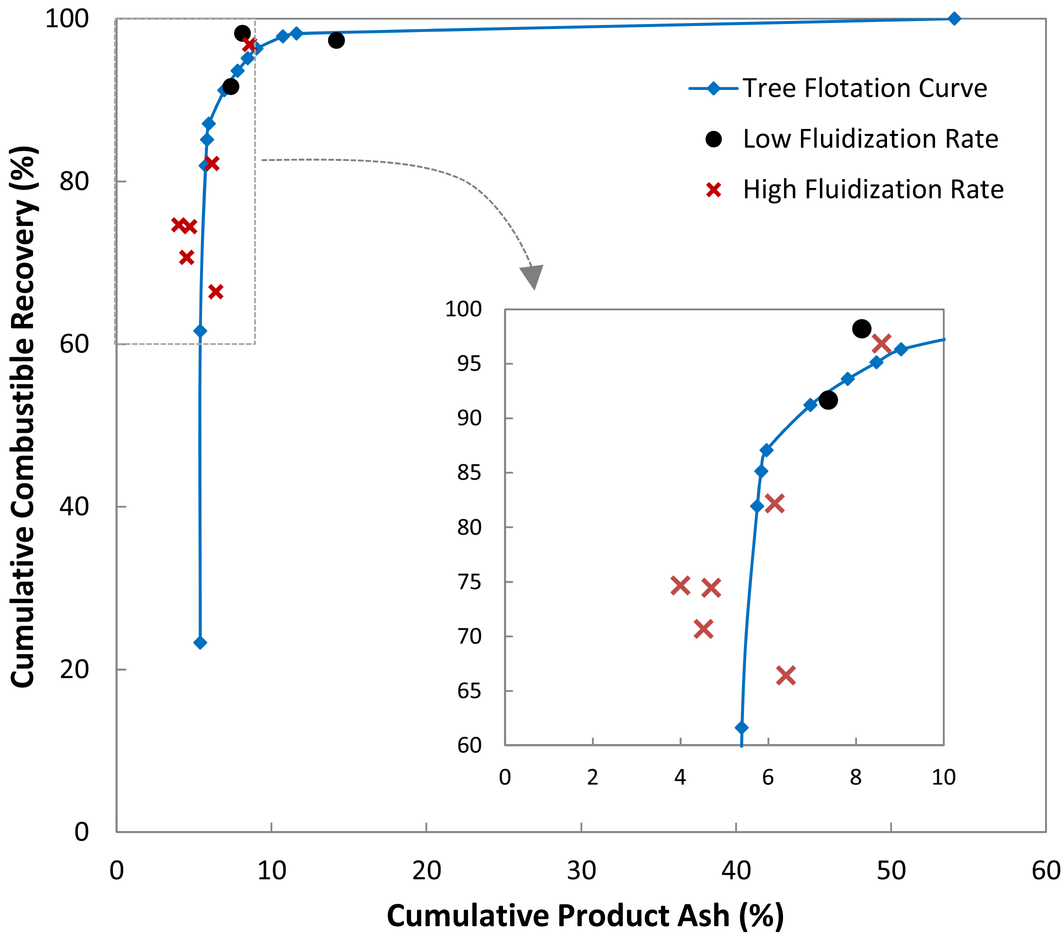

Figure 13: Comparison between the performance of the Reflux Flotation Cell and data generated from Tree Flotation analysis.

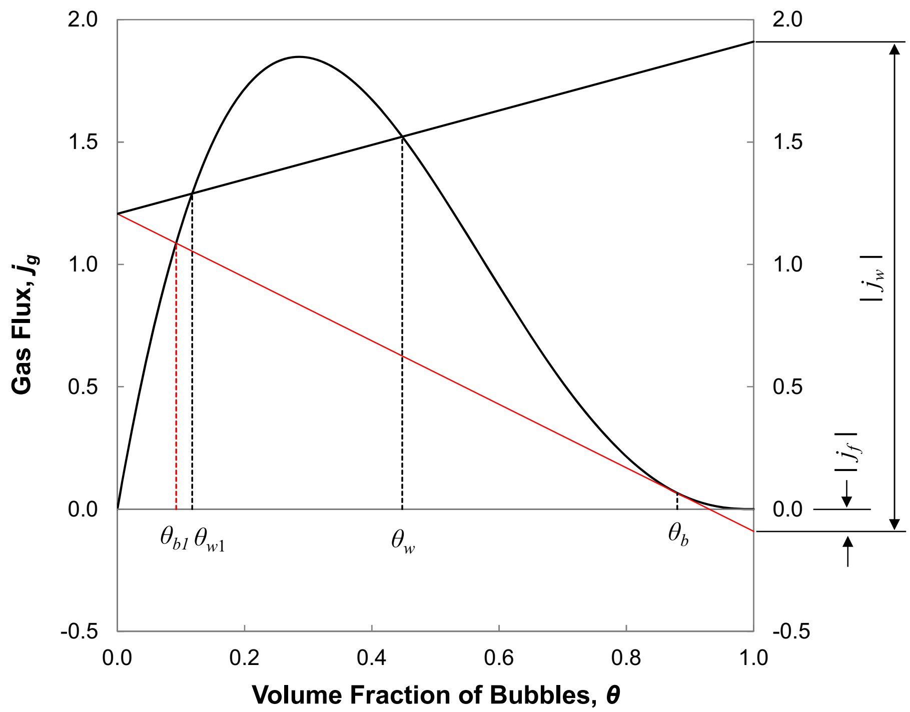

Figure A1: Drift Flux curve, $V_s\theta$, versus the volume fraction of bubbles, θ. The flux curve was constructed using the parameters V_t = 15 cm/s and n = 2.5. When j_g = 1.207 cm/s and j_w = 0 cm/s, two conjugate volume fractions, θ_b and θ_{b1} are formed, representing the volume fraction of bubbles in the foam and dilute bubbly zone, respectively. These values are obtained using the operating line that forms a tangent with the flux curve. When j_g = 1.207 cm/s and j_w = 2 cm/s, three conjugate volume fractions form in three distinct zones: (1) θ_b in the foam zone, (2) θ_w in the concentrated bubbly zone, and (3) θ_{w1} in the dilute bubbly zone. The additional volume fractions are obtained using the wash water operating line, with intercept on the right hand-side given by the bias flux.